



OPEN

Iron from nanostructured ferric phosphate: absorption and biodistribution in mice and bioavailability in iron deficient anemic women

Jeannine Baumgartner^{1,2,6}, Hans Christian Winkler^{1,6}, Lizelle Zandberg², Siriporn Tuntipopipat³, Phatchari Mankong³, Cor Bester⁴, Florentine Hilty¹, Jan Rijn Zeevaart^{4,5}, Sueppong Gowachirapant^{3✉} & Michael B. Zimmermann^{1✉}

Food fortification with iron nanoparticles (NPs) could help prevent iron deficiency anemia, but the absorption pathway and biodistribution of iron-NPs and their bioavailability in humans is unclear. Dietary non-heme iron is physiologically absorbed via the divalent metal transporter-1 (DMT1) pathway. Using radio-iron isotope labelling in mice with a partial knockdown of intestine-specific DMT1, we assessed oral absorption and tissue biodistribution of nanostructured ferric phosphate (FePO_4 -NP; specific surface area [SSA] $98 \text{ m}^2\text{g}^{-1}$) compared to ferrous sulfate (FeSO_4), the reference compound. We show that absorption of iron from FePO_4 -NP appears to be largely DMT1 dependent and that its biodistribution after absorption is similar to that from FeSO_4 , without abnormal deposition of iron in the reticuloendothelial system. Furthermore, we demonstrate high bioavailability from iron NPs in iron deficient anemic women in a randomized, cross-over study using stable-isotope labelling: absorption and subsequent erythrocyte iron utilization from two ^{57}Fe -labeled FePO_4 -NP with SSAs of $98 \text{ m}^2\text{g}^{-1}$ and $188 \text{ m}^2\text{g}^{-1}$ was 2.8-fold and 5.4-fold higher than from bulk FePO_4 with an SSA of $25 \text{ m}^2\text{g}^{-1}$ ($P < 0.001$) when added to a rice and vegetable meal consumed by iron deficient anemic women. The FePO_4 -NP $188 \text{ m}^2\text{g}^{-1}$ achieved 72% relative bioavailability compared to FeSO_4 . These data suggest FePO_4 -NPs may be useful for nutritional applications.

Iron deficiency anemia (IDA) is a major global health burden and women of childbearing age are particularly vulnerable¹. Iron fortification of foods is a recommended strategy to prevent IDA, but iron fortification remains a challenge, because well absorbed, water-soluble iron compounds, e.g. ferrous sulfate (FeSO_4), often cause unacceptable sensory changes when added to foods². Poorly acid-soluble iron compounds, such as ferric phosphate (FePO_4) in bulk form, are stable in foods but their absorption in humans is too low to have nutritional value³. However, the dissolution and absorption of poorly-soluble iron compounds is inversely related to particle size and nanostructured iron compounds may be useful as food fortificants or supplements⁴. We have previously shown that scalable nanostructured FePO_4 (FePO_4 -NP) produced by flame spray pyrolysis (FSP) dissolve rapidly in gastric conditions⁵. In an anemic rat model, iron bioavailability (determined as the ability to rapidly replete hemoglobin (Hb) when given orally) from two FePO_4 -NP compounds ($\text{FePO}_4/\text{Fe}_2\text{O}_3$, specific surface area [SSA] $197 \text{ m}^2/\text{g}$ and $\text{FePO}_4/\text{Zn}_3(\text{PO}_4)_2$, SSA $191 \text{ m}^2/\text{g}$) was 75 and 95%, respectively, compared to the ionic reference compound FeSO_4 ⁵. However, rodents absorb iron efficiently because they endogenously synthesize ascorbic acid, have lower duodenal pH, and are less affected by dietary absorption inhibitors than humans^{6,7}. Thus, whether the

¹Laboratory of Human Nutrition, Department of Health Sciences and Technology, ETH Zurich, Schmelzbergstrasse 7, 8092 Zurich, Switzerland. ²Center of Excellence in Nutrition, North-West University, Potchefstroom, South Africa. ³Institute of Nutrition, Mahidol University, Salaya, Nakhon Pathom 73170, Thailand. ⁴DST/NWU Preclinical Drug Development Platform, North-West University, Potchefstroom, South Africa. ⁵South African Nuclear Energy Corporation South Africa (Necsa), Pelindaba, South Africa. ⁶These authors contributed equally: Jeannine Baumgartner and Hans Christian Winkler. ✉email: sueppong.gow@mahidol.ac.th; michael.zimmermann@hest.ethz.ch

high bioavailability of FePO₄-NP determined in rats can be extrapolated to humans is unknown, since existing animal models were never validated with nano compounds.

Moreover, the mechanism of uptake of iron NPs from the gastrointestinal tract is uncertain. Ferrous iron from fortificants and foods is absorbed in the duodenum via the divalent metal transporter 1 (DMT1)^{2,8}. Ferric iron must be reduced to the ferrous state before uptake by DMT1^{9,10}. Since iron cannot be actively excreted in mammals and iron overload is toxic, iron absorption through DMT1 is tightly regulated by iron stores and circulating hepcidin¹¹. Because of their small size, iron NPs could be absorbed through other pathways^{12,13}, and unregulated translocation from the gut into body tissues might be toxic. In Caco-2 cell models, endocytosis of iron NPs has been described¹³, but siRNA-mediated knockdown of DMT1 reduced iron uptake from FePO₄-NP in Hutu-80 cell models by 50%¹⁴. Whether iron from FePO₄-NP can be absorbed independently of the DMT1 pathway *in vivo* remains uncertain.

Therefore, our study objectives were: (1) in mouse models, (i) to compare Hb trajectories (iron absorption and utilization) in intestine-specific DMT1 partial knockdown (DMT1^{int/int}) mice and homozygously floxed (DMT1^{fl/fl}) controls fed diets containing FePO₄-NP (SSA 98 m²g⁻¹) or FeSO₄ (positive reference compound) for 18 days; and (ii) to compare absorption and biodistribution of iron from a single oral dose of FePO₄-NP (SSA 98 m²g⁻¹) and FeSO₄ labelled with radioactive iron (⁵⁹Fe) in iron deficient anemic DMT1^{int/int} and DMT1^{fl/fl} control mice; (2) in iron deficient anemic women, to measure iron absorption and erythrocyte iron utilization (bioavailability) from a rice and vegetable meal fortified with large and small FePO₄-NP (SSA 98 m²g⁻¹ and 188 m²g⁻¹) labeled with a stable iron isotope (⁵⁷Fe), compared to ⁵⁸Fe-labeled bulk FePO₄ and FeSO₄ as negative and positive reference compounds, respectively.

Results

Iron nanoparticle production and characterization. Two different sized ferric orthophosphate dihydrate nanoparticles (FePO₄-NPs) with SSAs of 188 m²g⁻¹ and 98 m²g⁻¹ were produced by flame spray pyrolysis (FSP) at ETH Zurich as previously described¹⁵ with adaptations (see “Methods”). FSP is a scalable production process¹⁶ for tailor-made particles with high SSA and well-defined chemical composition¹⁷. As indicated by transmission electron microscopy (TEM) images and X-ray diffraction (XRD), the two FePO₄-NPs are almost spherical particles with a calculated size (dBET) of 11 nm and 21 nm, respectively (Fig. 1a-c) and XRD-amorphous (Fig. 1d). Amorphous ferric orthophosphate with a SSA of 25 m²g⁻¹ served as reference compound for BET and XRD measurements. FePO₄-NPs for the human study were produced from stable isotope (⁵⁷Fe) enriched precursors, bulk FePO₄ and FeSO₄ from (⁵⁸Fe) enriched precursors. For the human study, bulk size FePO₄ with a SSA of 27 m²g⁻¹ was produced as previously described¹⁸ with adaptations (see “Methods”). As indicated by TEM, these particles have a size above 100 nm and an irregular shape. The calculated primary particle size of these FePO₄ particles with an SSA of 27 m²g⁻¹ would be 77 nm; however, as shown in the TEM images, the assumption of sphericity is not valid and we therefore refer to these particles as bulk FePO₄. For the methods of SSA, hydrodynamic diameter, XRD and TEM, see “Methods”. In ultrapure water, bulk FePO₄ and the 98 m²g⁻¹ and 188 m²g⁻¹ FePO₄-NPs formed large agglomerates with a mean diameter and polydispersity index (PDI) of 859 ± 152 nm (PDI 0.63) at pH 6.7, 1191 ± 603 nm (PDI 0.34) at pH 6.1 and 1149 ± 132 nm (PDI 0.41) at pH 6.0 and a Zeta potential of -5.3 ± 1.6 mV, -2.1 ± 0.1 mV and -2.5 ± 0.1 mV. The same FePO₄-NPs were shown to form stable agglomerates for up to 72 h in aqueous dispersions with added protein content (10% FCS) with a mean diameter of 231–615 nm¹⁹. Particle characterization followed MIRIBEL guidelines²⁰.

Characterization of intestine-specific DMT1 knockdown model. We chose DMT1^{int/int} and DMT1^{fl/fl} littermates (controls) as the model to study absorption and biodistribution of nanosized FePO₄ (SSA 98 m²g⁻¹). DMT1^{int/int} and DMT1^{fl/fl} mice were bred on a C57BL/6 background by crossing floxed DMT1 (courtesy of Nancy Andrews, Duke University, USA²¹) with villin-Cre transgenic mice. Figure 2a shows a schematic illustration of the floxed allele and the primer positions used for genotyping of the DMT1^{int/int} and DMT1^{fl/fl} mice. Homozygously floxed DMT1^{fl/fl} mice that do not carry the Cre recombinase were chosen as controls in all mice experiments to account for a potential effect of floxing on iron absorption and biodistribution. For details of breeding, genotyping and housing see “Methods”.

To validate the model and to determine the optimal age window for the feeding and radio-isotope experiments, we assessed Hb concentration trajectories of DMT1^{int/int} and DMT1^{fl/fl} mice fed an iron-sufficient (35 ppm iron as ferrous citrate) or iron deficient (3 ppm native iron) diet from postnatal day (PND) 24 (weaning) until 42. PND 42 was set as endpoint, as it was the age when first mice reached a Hb < 4 g/dL, which we defined as the humane endpoint (see “Methods” for definition)²². We measured Hb in tail blood spots at PND 24, 27, 30, 33, 36, 39, and 42. Using repeated-measures ANOVA with time as within-group factor, and dietary iron content (35 ppm vs. 3 ppm) and genotype (DMT1^{int/int} vs. DMT1^{fl/fl}) as between-group factors, we found a significant effect of iron content (p = 0.023) for lower Hb in mice receiving the 3 ppm iron diet, and of genotype (p = 0.006) for lower Hb in DMT1^{int/int} mice (Fig. 2b). There was no significant iron content x genotype interaction, indicating that both the 3 ppm iron diet and the intestine-specific DMT1 knockdown independently lowered Hb across PND 24–42. However, we obtained no significant time x iron content (p = 0.087) or time x genotype (p = 0.090) interactions, indicating that the Hb-lowering effect of the 3 ppm diet and the intestine-specific DMT1 knockdown was not time-dependent during this age period. These results confirm that the DMT1^{int/int} mice bred for our studies have significantly lower Hb concentrations from PND 24–42, both when fed an iron-sufficient or iron deficient diet, but there was no progressive decline in Hb concentrations, suggesting upregulation of iron absorption from a partly intact DMT1 pathway.

We further determined expression of DMT1 mRNA harboring an iron-responsive element (IRE) in its 3'-terminal exon and the upstream 5' exon1A in crude homogenates prepared from whole duodenum (not isolated

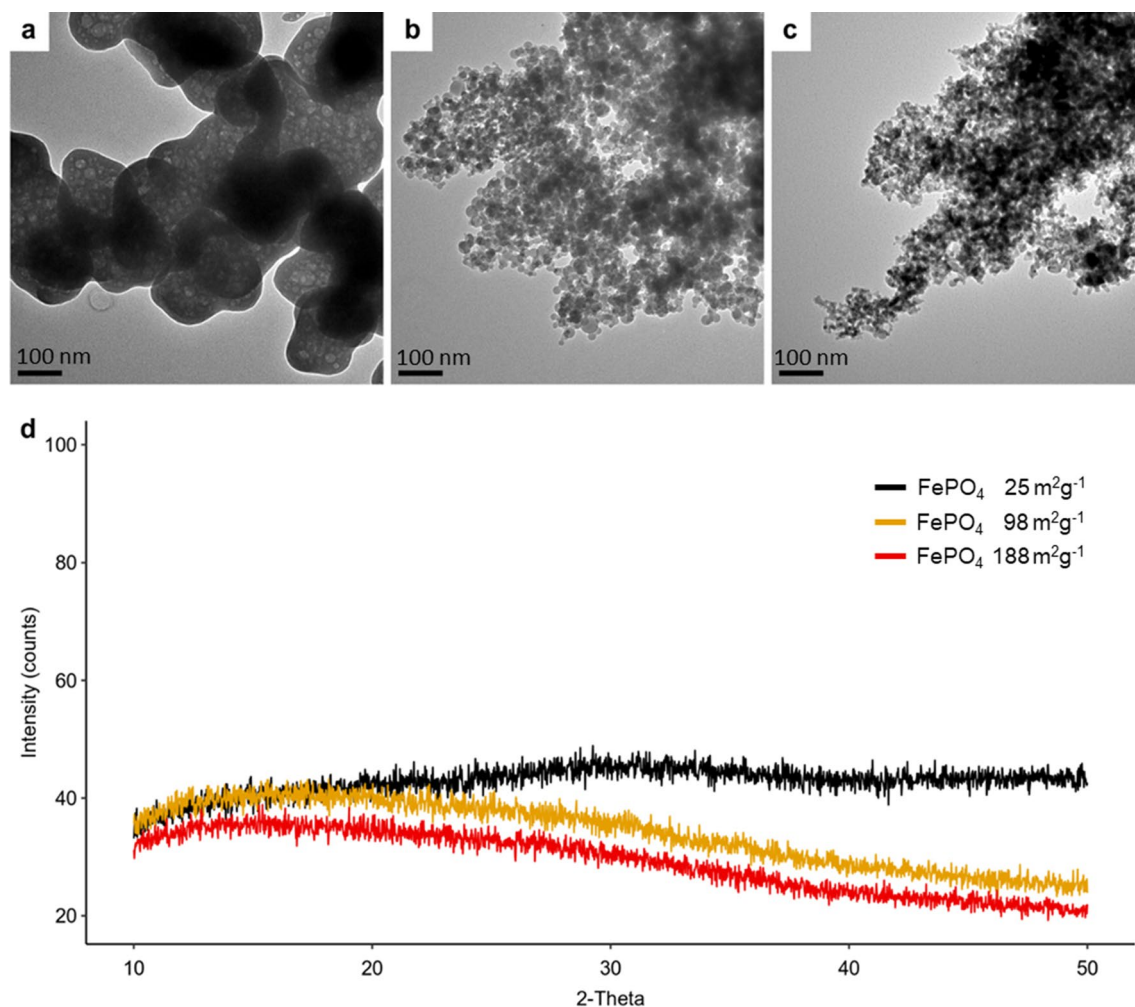


Figure 1. Particle characterization. (a–c) TEM micrographs of (a) bulk FePO₄, (b) 98 m² g⁻¹ FePO₄ and (c) 188 m² g⁻¹ FePO₄, scale bars: 100 nm. (d) XRD patterns of 25 m² g⁻¹, 98 m² g⁻¹ and 188 m² g⁻¹ FePO₄. The absence of peaks in the X-ray diffraction (XRD) analysis indicates that all compounds were XRD amorphous. X-axis indicates the diffraction angle (2-Theta), Y-axis indicates the counts.

enterocytes), colon and liver of DMT1^{int/int} and DMT1^{fl/fl} mice fed an iron deficient diet from PND 24–42 (Fig. 2c). The DMT1-IRE and DMT1-exon1A isoforms were previously implicated in iron regulation, specifically in the duodenum²³. DMT1 mRNA levels are expected to be increased in the duodenum of iron deficient mice with a functional DMT1 gene²³. We showed that expression of both exon1A and the IRE of DMT1 was significantly lower in the duodenum of DMT1^{int/int} compared to DMT1^{fl/fl} mice fed an iron deficient diet. However, the reduction in DMT1 mRNA expression was partial, suggesting incomplete knockdown of DMT1 in the DMT1^{int/int} mice. This is supported by the observation that expression of the DMT1-IRE isoform in the duodenum was positively associated with Hb concentrations measured at PND42 in DMT1^{fl/fl} mice receiving 3 ppm and 35 ppm iron (standardized $\beta = 0.623$, $p = 0.026$; regression models controlled by sex), with the same trend observed in DMT1^{int/int} mice (standardized $\beta = 0.522$, $p = 0.079$) (data not shown). There were no differences in expression of DMT1 mRNA between DMT1^{int/int} and DMT1^{fl/fl} mice in colonic and liver tissue, confirming the intestine-specificity of the partial knockdown.

Eighteen-day FePO₄-NP feeding study in DMT1^{int/int} and DMT1^{fl/fl} mice. To determine whether FePO₄-NP is absorbed via DMT1 and utilized for erythropoiesis, we compared Hb trajectories between DMT1^{int/int} and DMT1^{fl/fl} (control) mice fed with FePO₄-NP (SSA 98 m² g⁻¹) or FeSO₄ as the reference compound from PND 24–42 (18 days). We hypothesized that (1) intestine-specific DMT1 knockdown would lower Hb equally in mice fed FePO₄-NP or FeSO₄ and, (2) that Hb would be comparable in DMT1^{fl/fl} mice fed iron in the form of nanosized FePO₄-NP or FeSO₄. We randomly allocated a total of 28 male and female DMT1^{int/int} and DMT1^{fl/fl} mice to receive either the purified AIN-93G diet containing 35 ppm iron as FePO₄-NP or FeSO₄ from PND 24–42. The design of the study is shown in Fig. 3a. For more details see “Methods”. We measured Hb in tail blood spots at PND 24, 27, 30, 33, 36 and 42. Using repeated-measures ANOVA with age as within-group factor, and iron compound (FePO₄-NP vs. FeSO₄) and genotype (DMT1^{int/int} vs. DMT1^{fl/fl}) as between-group factors,

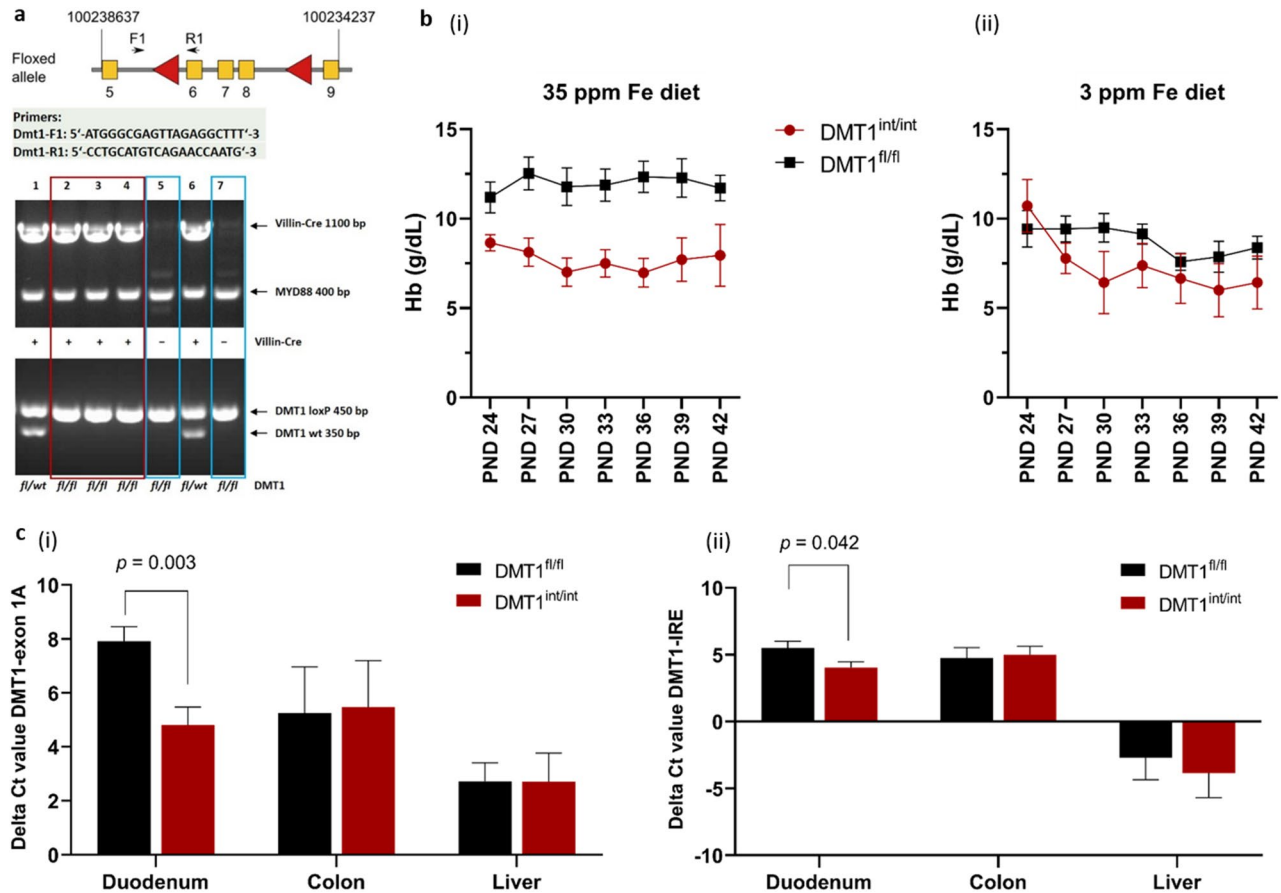


Figure 2. Characterization of the DMT1^{int/int} mouse model. **(a)** Schematic illustration of the floxed allele and primer positions used to confirm excision by PCR genotyping of intestine knockdown (DMT1^{int/int}, lane 2–4, red box) and control (DMT1^{fl/fl}, lane 5 and 7, blue boxes) mice. Image was cropped and compiled from original images available as Supplementary Figs. 1 and 2. **(b)** Haemoglobin (Hb) trajectory (PND 24–42) in DMT1^{int/int} (n = 6 male; n = 4 female) and DMT1^{fl/fl} (n = 10 male; n = 11 female) mice receiving the AIN93G diet containing (i) 35 ppm iron (as ferrous citrate) and (ii) 3 ppm iron (native). Results are shown as means ± SEM. **(c)**, Expression of (i) DMT1-exon1A and (ii) DMT1-IRE mRNA in duodenum, colon and liver of 42-day-old DMT1^{int/int} and DMT1^{fl/fl} mice fed an iron deficient (3 ppm iron) diet from PND 24–42, normalized to 18S and βActin as endogenous reference genes to calculate delta Ct values. Differences in gene expression by genotype (DMT1^{int/int} vs. DMT1^{fl/fl}) were determined by two-sided independent t-tests. The results are shown as means ± SEM and differences were considered significant at p < 0.05.

we found a significant effect of genotype ($p=0.042$) for lower Hb concentrations in DMT1^{int/int} mice, and a nonsignificant effect of iron compound ($p=0.067$) for lower Hb in mice fed FePO₄-NP (Fig. 3b). Although the interaction between genotype and iron compound was not significant ($p=0.140$), the Hb-lowering effect of the DMT1 knockdown appeared to be compound-specific, in that Hb trajectories were similar between compounds in DMT1^{fl/fl} mice, but Hb concentrations were lower in DMT1^{int/int} mice fed FePO₄-NP than fed FeSO₄. The data in Fig. 3b suggest the FeSO₄ was nearly as effective at increasing Hb in DMT1^{int/int} mice as it was in DMT1^{fl/fl} mice, whereas for FePO₄-NP, Hb concentrations were increased in the DMT1^{fl/fl} mice but were unchanged in the DMT1^{int/int} mice. This pattern is supported by the liver iron concentrations (Fig. 3c) at PND 42 in DMT1^{int/int} and DMT1^{fl/fl} mice fed FePO₄-NP or FeSO₄. We found a significant effect of genotype ($p=0.009$) for lower liver iron concentrations in DMT1^{int/int} mice. Specifically, FePO₄-NP feeding resulted in significantly lower liver iron concentrations in DMT1^{int/int} compared to DMT1^{fl/fl} mice, but FeSO₄ did not. The lacking effect of the intestinal DMT1 knockdown on Hb trajectories and liver iron concentrations in mice fed a diet containing iron as FeO₄-NP may be explained by the high solubility of FeSO₄ at low gastric pH and rodents' high efficiency in absorbing iron^{6,7}. Considering that our model was not a complete intestinal DMT1 knockout model (described above), it can be speculated that rapid dissolution in the proximal gut and absorption of FeSO₄ in mice with a partial intestinal DMT1 knockdown was enough to maintain erythropoiesis and liver iron stores during the experimental period (PND 24–42). This may also explain why the DMT1^{int/int} mice fed (and bred on) ferrous citrate in the characterization experiment were more anemic from PND 24–42 than the DMT1^{int/int} mice fed (and bred on) FeSO₄ in the feeding experiment. Taken together, these data suggest that compared to FeSO₄, FePO₄-NP were less well absorbed in DMT1^{int/int} compared to DMT1^{fl/fl} mice, suggesting that absorption of iron from FePO₄-NP is more sensitive to partial knockdown of DMT1.

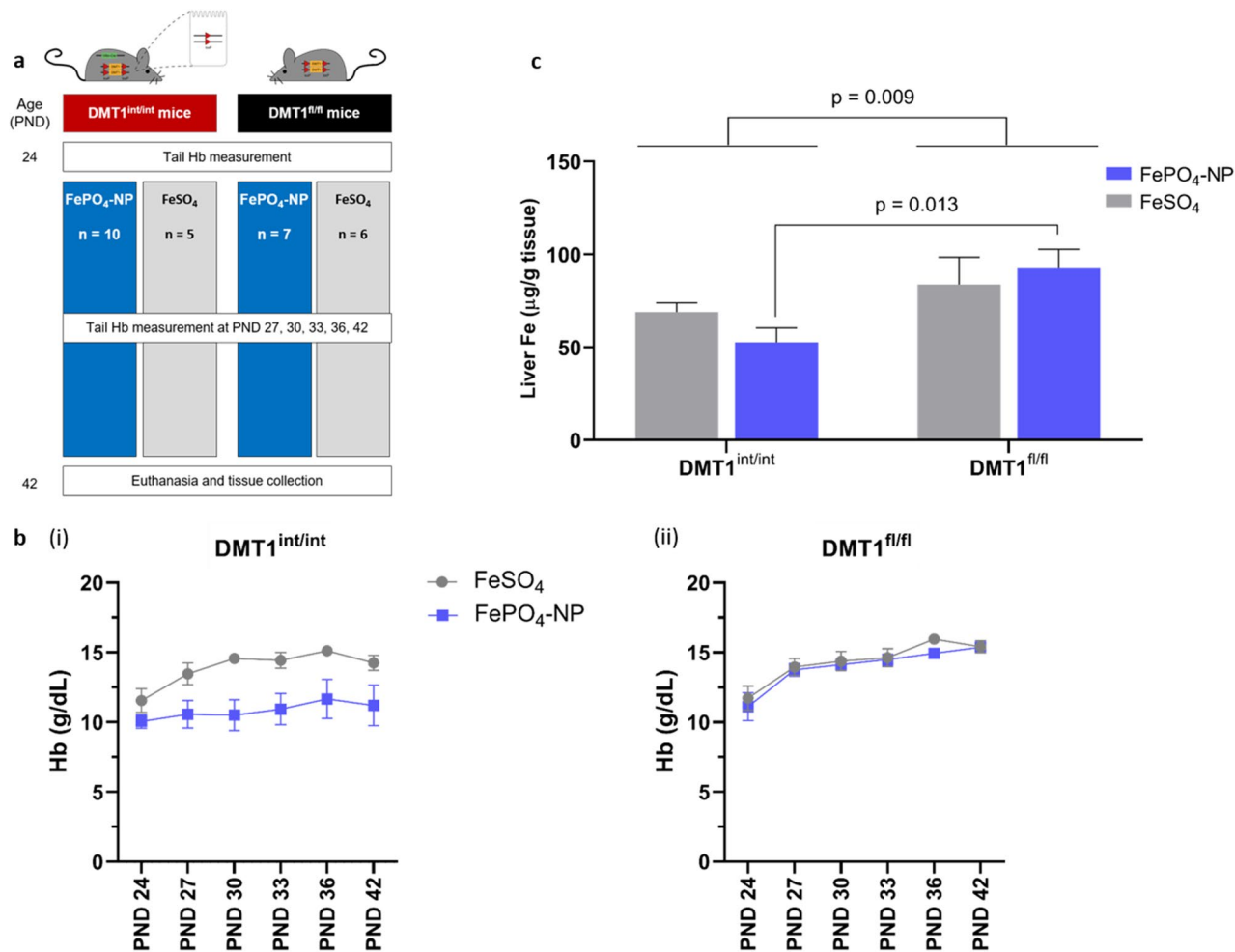


Figure 3. Eighteen-day feeding study in DMT1^{int/int} and DMT1^{fl/fl} mice. **(a)** Outline of feeding study. **(b)** Hemoglobin (Hb) trajectory in **(i)** DMT1^{int/int} (n = 6 male; n = 9 female) and **(ii)** DMT1^{fl/fl} (n = 6 male; n = 7 female) mice receiving the AIN93G diet fortified with FePO₄-NP (SSA 98 m²g⁻¹) or FeSO₄ (reference compound). Results are shown as means ± SEM. **(c)** Liver iron concentrations in DMT1^{int/int} and DMT1^{fl/fl} mice fed diets fortified with 35 ppm FeSO₄ or FePO₄-NP for 18 days (postnatal days [PND] 24–42). Differences in liver iron concentrations by genotype (DMT1^{int/int} vs. DMT1^{fl/fl}) and by iron compound (FePO₄-NP vs. FeSO₄) were determined by two-sided independent t-tests. The results are shown as means ± SEM and differences were considered significant at p < 0.05.

Absorption and biodistribution of radiolabeled FePO₄-NP and FeSO₄ from a single oral dose in iron deficient anemic DMT1^{int/int} and DMT1^{fl/fl} mice. To determine whether absorption of FePO₄-NP is DMT1-dependent and biodistribution comparable to FeSO₄ in iron deficient anemic conditions, we administered a single oral dose of irradiated FePO₄-NP (SSA 98 m²g⁻¹) or FeSO₄ labelled with radioactive iron (⁵⁹Fe) to iron deficient anemic DMT1^{int/int} and DMT1^{fl/fl} control mice and measured tissue distribution of ⁵⁹Fe 24 h after administration. Based on the findings from the feeding study, we hypothesized that less iron from a single oral dose of FePO₄-NP would be absorbed in DMT1^{int/int} than DMT1^{fl/fl} mice. We further hypothesized that tissue distribution of iron taken up and absorbed from the single oral dose of FePO₄-NP would be equal to FeSO₄ in both iron deficient anemic DMT1^{int/int} and DMT1^{fl/fl} control mice. A total of 27 male and female DMT1^{int/int} and DMT1^{fl/fl} mice were randomly allocated by genotype to receive radiolabeled FePO₄-NP (SSA 98 m²g⁻¹) or FeSO₄ and were placed on an iron deficient diet (3 ppm native iron) from PND 21 until the end of the experiment. At PND 24, mice were transported to the Nuclear Energy Corporation South Africa (NECSA) and acclimatized until administration of radiolabeled FePO₄-NP or FeSO₄ by oral gavage at PND 30. The design of the study is shown in Fig. 4a. The day before compound administration, Hb was measured in a tail blood spot, and 2 h before administration mice were fasted. A single dose of ~50 µg iron (mean ± SEM administered: 47.4 ± 2.9 µg) in the form of the allocated compound labelled with ⁵⁹Fe (FePO₄-NP: 0.08 ± 0.01 MBq; FeSO₄: 0.52 ± 0.2 MBq) was orally gavaged (in 100 µL saline containing 0.1% bovine serum albumin) and total dose administered determined by measuring syringe activity before and after gavage using a dose calibrator (Capintec CRC-15R, Capintec Inc., Ramsey, NJ, USA). Mice were then placed into a clean metabolic cage and received ad libitum access to iron deficient diet (3 ppm iron) one hour after oral gavage. After 24 h, mice were euthanized and individual

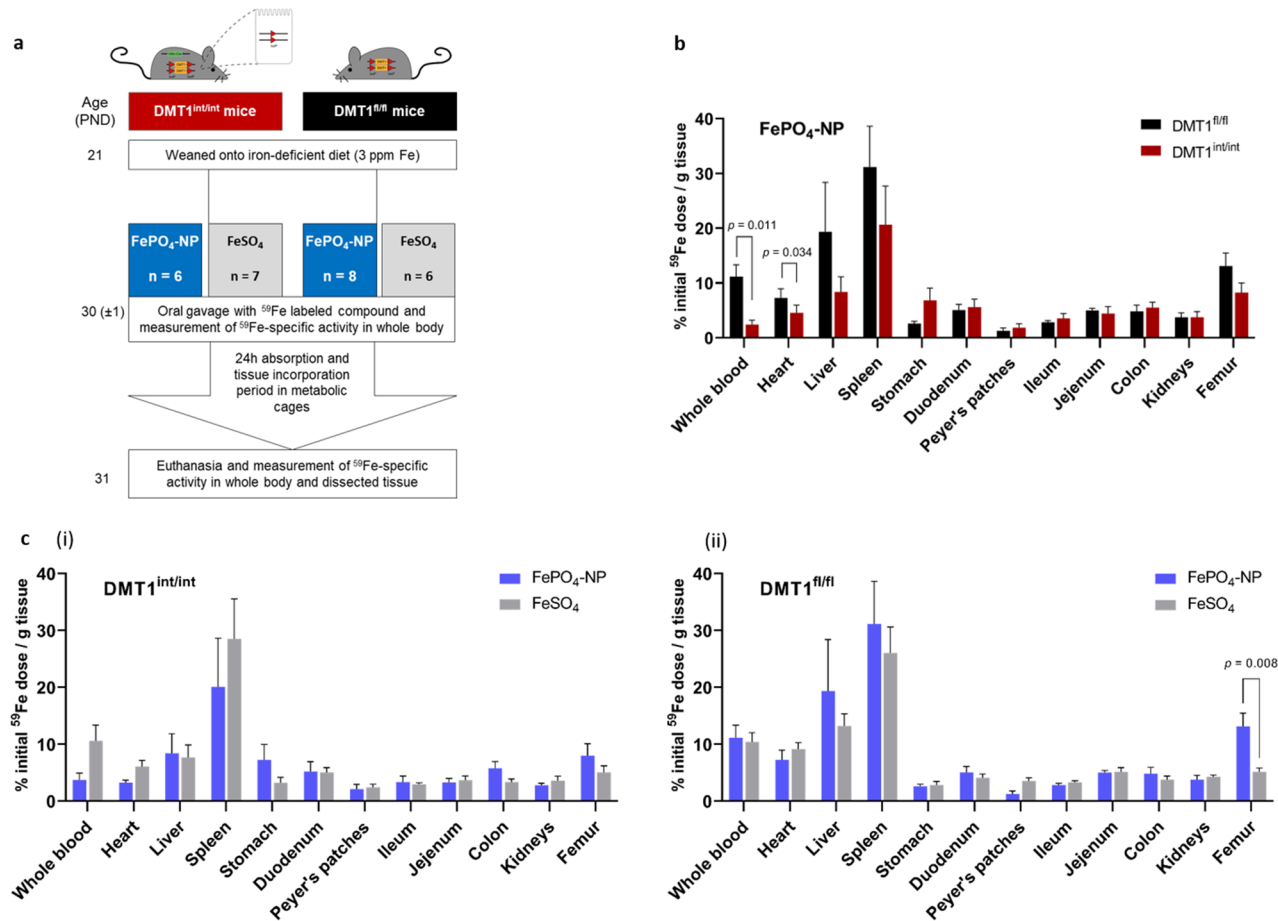


Figure 4. Absorption and biodistribution of a single oral dose of radiolabeled FePO₄-NP and FeSO₄ iron deficient anemic DMT1^{int/int} and DMT1^{fl/fl} mice. (a) Outline of radioisotope study. (b) Biodistribution of ⁵⁹Fe (% of initial ⁵⁹Fe/g tissue) from a single dose (~50 µg) of FePO₄-NP (SSA 98 m² g⁻¹) after oral gavage in iron deficient anemic DMT1^{fl/fl} (n = 7 male; n = 5 female) and DMT1^{int/int} (n = 7 male, n = 8 female) mice. Differences in tissue ⁵⁹Fe distribution by genotype (DMT1^{int/int} vs. DMT1^{fl/fl}) were determined by two-sided independent t-tests. The results are shown as means ± SEM and differences were considered significant at p < 0.05. (c) Biodistribution of ⁵⁹Fe from FePO₄-NP and FeSO₄ (reference compound) 24 h after oral gavage in iron deficient anemic (i) DMT1^{int/int} mice and (ii) DMT1^{fl/fl} mice. Differences in tissue ⁵⁹Fe distribution by iron compound (FePO₄-NP vs. FeSO₄) were determined by two-sided independent t-tests. The results are shown as means ± SEM and differences were considered significant at p < 0.05.

tissues were dissected and analyzed for ⁵⁹Fe content using a gamma-counter. All counts were adjusted for decay. For more details see “Methods”.

DMT1^{int/int} mice had significantly lower Hb than DMT1^{fl/fl} mice (5.7 ± 0.5 vs. 8.9 ± 0.7 g/dL, p = 0.01) the day before compound administration. As shown in Fig. 4b, 24 h after administration, significantly less ⁵⁹Fe from FePO₄-NP was present in whole blood and heart (expressed as % initial ⁵⁹Fe dose/g tissue) in DMT1^{int/int} compared to DMT1^{fl/fl} mice. These data are consistent with lower absorption of FePO₄-NP in DMT1^{int/int} compared to DMT1^{fl/fl} mice shown in the feeding study above (Fig. 3b,c). Notably, in DMT1^{int/int} and DMT1^{fl/fl} mice (Fig. 4c), we found no significant difference in tissue ⁵⁹Fe distribution between FePO₄-NP and FeSO₄. The only exception was in DMT1^{fl/fl} mice, where significantly more ⁵⁹Fe from FePO₄-NP was present in femoral bone marrow than from FeSO₄ (Fig. 4c,ii). Overall, the results from this study indicate that in iron deficient anemic mice, iron from a single oral dose of FePO₄-NP displays a similar biodistribution as FeSO₄.

Iron bioavailability of two ⁵⁷Fe-labeled FePO₄-NP in iron deficient anemic women. To quantify iron absorption and erythrocyte incorporation (bioavailability) from two FePO₄-NPs (SSA of 98 m² g⁻¹ and 188 m² g⁻¹) in iron deficient, mostly anemic women, we fortified two standardized rice test meals with FePO₄-NPs labeled with stable iron isotopes and compared their performance to labeled bulk FePO₄ with a SSA of 25 m² g⁻¹ (as the negative reference compound) and dried FeSO₄ (as the positive reference compound) in a randomized, cross-over study. We hypothesized that: (1) an increase in SSA of the FePO₄-NP compound would significantly increase iron bioavailability, and (2) iron bioavailability from FePO₄-NP SSA 188 m² g⁻¹ would not differ significantly compared to iron bioavailability from FeSO₄. Iron bioavailability was estimated by using stable-isotope techniques measuring the incorporation of ⁵⁷Fe and ⁵⁸Fe into erythrocytes 14 days after administration²⁴.

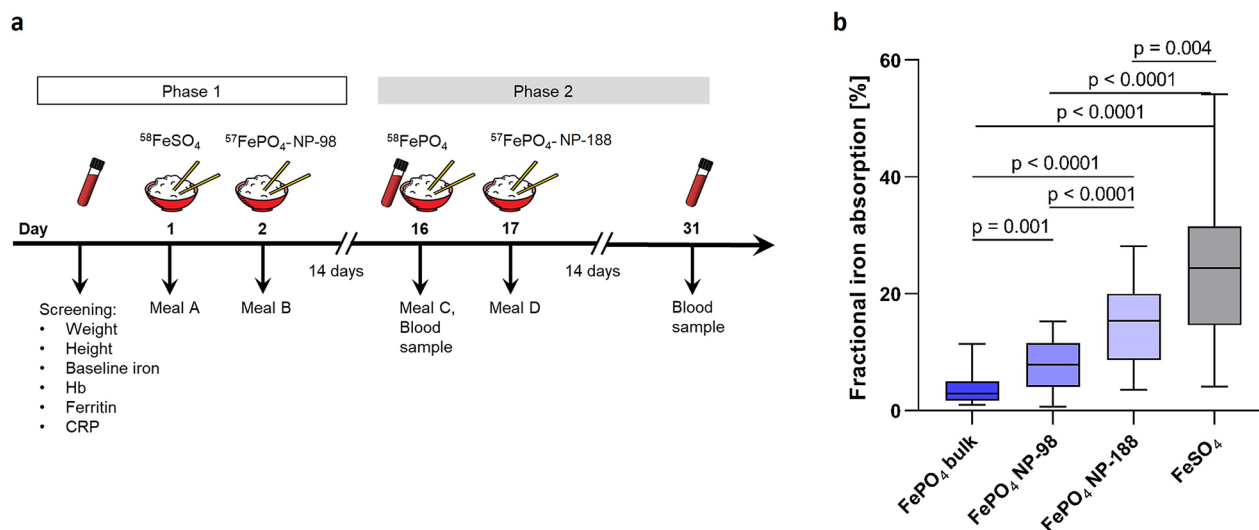


Figure 5. Iron bioavailability of two ^{57}Fe -labeled FePO_4 -NP in iron deficient anemic women ($n = 18$). **(a)** Outline of randomized cross-over study. **(b)** Fractional iron absorption (%) from rice test meals fortified with FePO_4 -NPs (SSA $98 \text{ m}^2 \text{ g}^{-1}$ and $188 \text{ m}^2 \text{ g}^{-1}$) labeled with a stable isotope (^{57}Fe), and ^{58}Fe -labeled bulk FePO_4 (SSA $25 \text{ m}^2 \text{ g}^{-1}$) and FeSO_4 as negative and positive reference compounds, respectively. Meal sequence was randomized across all women. Pairwise comparisons were performed using two-sided paired t-tests with Bonferroni adjustment for multiple testing. Boxes indicate median and interquartile ranges, whiskers describe the range of the data (min to max). Differences were considered significant at $p < 0.05$. CRP C-reactive protein, Hb hemoglobin.

The study was carried out in 18 Thai women who provided informed written informed consent. Main inclusion criteria were: (1) female aged 18 to 49 years and (2) $\text{Hb} \geq 80 \text{ g/L}$ and plasma ferritin $< 25 \mu\text{g/L}$ (see “Methods” for additional inclusion criteria and details on methods). We chose Thailand as our study site because, worldwide, the greatest number of women with anemia live in the WHO South and Southeast Asia Region, and in Thailand, 32% of women of reproductive age are anemic²⁵. The study had a cross-over design in which all women consumed four labeled test meals over a 31-day period (Fig. 5a). The order of the four test meals was randomly assigned to each subject. In a first phase, the women presented fasting and consumed the first test meal between 7.00 and 9.00 am on day 1 and the second test meal between 7.00 and 9.00 am on days 16 and 17. Consumption of meals was directly supervised and all women completed all meals. No intake of food and fluids was allowed for 2 h afterward. The standardized test meal consisted of rice with vegetables (see “Methods”) fortified with 2 mg of isotopically labeled compound and a glass of deionized water (200 ml). The two FePO_4 -NPs were labeled with ^{57}Fe , while the bulk FeSO_4 and FePO_4 were labeled with ^{58}Fe (see “Methods”). We calculated the amounts of ^{57}Fe and ^{58}Fe labels in blood 14 d after the 2nd and 4th test meals based on the shift in iron-isotopic ratios and the estimated amount of iron circulating in the body²⁴. For details of laboratory analyses, calculation of iron absorption and statistical analyses see “Methods”.

Baseline characteristics of the 18 women are shown in Table 1; 14 were iron deficient, 12 had iron deficiency anemia, 15 had normal hemoglobin A (HbA) and three had HbE trait. As shown in Fig. 5b, median (interquartile range [IQR]) fractional iron absorption was 2.87 (1.71–5.02), 7.90 (4.06–11.52), 15.37 (8.63–20.0) and 24.37 (14.64–31.50) from the test meals fortified with bulk FePO_4 , FePO_4 -NP SSA $98 \text{ m}^2 \text{ g}^{-1}$, FePO_4 -NP SSA $188 \text{ m}^2 \text{ g}^{-1}$, and FeSO_4 , respectively, with significant differences between all groups (for all, $p < 0.005$). Thus, particle size reduction of FePO_4 to SSA $98 \text{ m}^2 \text{ g}^{-1}$ and $188 \text{ m}^2 \text{ g}^{-1}$ increased iron bioavailability 2.8 and 5.4-fold compared to bulk FePO_4 , and achieved a relative bioavailability of 34% and 72% compared to FeSO_4 . In separate linear regressions including C-reactive protein and plasma ferritin (iron status) as independent variables and iron absorption from bulk FePO_4 and FeSO_4 combined (standardized $\beta = -0.393$, $\text{SE} = 0.008$, $p = 0.075$) and on iron absorption from the two FePO_4 -NPs combined (standardized $\beta = -0.575$, $\text{SE} = 0.014$, $p = 0.0027$) as outcome variables, plasma ferritin was a stronger negative predictor of iron absorption from the two FePO_4 -NPs ($p = 0.007$) than from the larger compounds ($p = 0.027$). Because iron absorption through the usual DMT1 mediated pathway is regulated by iron status¹⁰, but absorption through simple translocation of nanoparticle iron would likely not be, this is consistent with iron absorption from FePO_4 -NPs being at least partially dependent on the DMT1 mediated pathway.

Conclusions

Previous *in vitro* studies suggested that gastrointestinal uptake of iron NPs could occur through several mechanisms^{13,26,27}. Our *in vivo* data suggest that absorption of FePO_4 -NPs is largely DMT1 dependent (Fig. 3). Supporting our findings, uptake in cell models of the same FePO_4 -NP SSA $188 \text{ m}^2 \text{ g}^{-1}$ used in this study was reduced by DMT1 inhibitors or siRNA targeting of DMT1¹⁴. However, our findings do not rule out a DMT1 independent route for absorption of NP iron, as our $\text{DMT1}^{\text{int/int}}$ mice had reduced but still detectable expression

n	18
Age ^a , years	31.3 ± 7.3
Body weight, kg	51.7 ± 5.3
BMI, kg/m ²	20.5 ± 1.4
Hemoglobin ^b , g/L	11.5 (9.8–12.4)
Plasma ferritin, µg/L	8.5 (5.0–16.8)
Soluble transferrin receptor, mg/L	7.4 (5.6–10.9)
C-reactive protein, mg/L	1.0 (0.5–2.4)
α-1-acid glycoprotein, g/L	0.49 (0.42–0.52)
Inflammation, n (%)	2 (11)
Anemia, n (%)	14 (78)
Iron deficiency, n (%)	14 (78)
Iron deficiency anemia, n (%)	12 (67)

Table 1. Baseline characteristics of the Thai women (n = 18) participating in the iron absorption study. ^aMean ± standard deviation (all such values). ^bMedian; interquartile ranges in parentheses (all such values).

of DMT1-exon 1A and DMT1-IRE in the duodenum and this partial knockdown did not affect absorption of the reference compound FeSO₄ during the experimental period (PND 24–42). We did not determine the expression of other DMT1 isoforms, which could have been responsible for the observed iron absorption, nor measure DMT1 protein levels in duodenal enterocytes to confirm the absence of DMT1 in DMT1^{int/int} knockdown mice. Importantly, our mouse data (Fig. 4) suggest that the biodistribution of FePO₄-NPs after uptake in anemic DMT1^{int/int} and DMT1^{fl/fl} mice is comparable to FeSO₄, and there was no abnormal tissue deposition of iron absorbed from FePO₄-NP in the reticuloendothelial system (spleen, Peyer's Patches) or in the kidney or liver. In our human study, plasma ferritin was a strong negative predictor of iron absorption from the two FePO₄-NPs (SSA of 188 m² g⁻¹ and 98 m² g⁻¹), suggesting physiologic regulation by body iron stores. Taken together, these data argue against, but do not rule out, unregulated translocation and biodistribution of NP iron from gastrointestinal exposure.

Other food-relevant nanoparticles, e.g. SiO₂, TiO₂, ZnO and Al₂O₃, induce adverse effects in human intestinal cells or experimental animals^{28–37}. In contrast, gastrointestinal exposure to a variety of iron NPs has not been associated with measurable toxicity^{5,19,26,38–44}. Short-term feeding of iron deficient rats with diets containing iron NPs^{5,38} or iron NPs stabilized on β-lactoglobulin fibrils⁴³ did not cause histopathology or oxidative stress. We previously performed extensive toxicity testing of the FePO₄ NPs used in this study¹⁹. In rats fed diets containing these iron NPs for 90 days (at doses at which FeSO₄ has been shown to induce adverse effects), feeding did not cause toxicity, including oxidative stress, organ damage, abnormal tissue iron accumulation or histological changes¹⁹. Furthermore, they were taken up in vitro by gastrointestinal cells without reducing cell viability or inducing oxidative stress¹⁹. In these studies, FePO₄ nanoparticles appeared to be as safe for ingestion as FeSO₄.

Conflicting information regarding the toxicity of food relevant nanoparticles and regulatory issues have so far hampered applications of nanotechnology in the food sector. However, as described above, in vitro and in vivo studies have consistently shown that iron NPs do not show measurable toxicity on gastrointestinal exposure. Here, we demonstrate that absorption of FePO₄-NPs is largely via the physiological DMT1 pathway and biodistribution patterns resemble FeSO₄. In addition, we show that nanostructuring of FePO₄ sharply increases bioavailability in anemic women and achieves a relative bioavailability of 72% compared to FeSO₄, confirming previous absorption data in rats^{5,38}. Together, these findings suggest the promise of iron NPs as novel food fortificants. However, further research is needed to better clarify the uptake pathways of iron and other mineral NPs from gastrointestinal exposure before they can be recommended for nutritional applications.

Methods

Nanoparticle production and characterization. For the production of nanostructured ferric phosphate (FePO₄-NP) by flame spray pyrolysis (FSP), iron nitrate nonahydrate (purity ≥ 97.0%, Sigma-Aldrich, Buchs, Switzerland) and tributyl phosphate (97%, Sigma-Aldrich) were dissolved in a 1:1 mixture by volume of ethanol (denat. 2% 2-butanone, Alcosuisse) and 2-ethylhexanoic acid (purity ≥ 99%, Sigma-Aldrich) at a total metal concentration of 0.4 mol L⁻¹ or 0.5 mol L⁻¹ for the two compounds. This precursor solution was fed at 2 or 7 mL min⁻¹ into the FSP spray nozzles by a syringe pump (Lambda, VIT-FIT) and atomized by co-flowing 5 or 7 L min⁻¹ of oxygen (purity ≥ 99.5%, Pangas) at 1.5 bar pressure drop. The spray was ignited by a methane/oxygen (2.5 L min⁻¹) ring-shaped flame⁴⁵. Using a vacuum pump (Busch, Mink MM1202 AV), product particles were collected on water-cooled Teflon membrane-filters (1TMTF700WHT, BHA Technologies AG) placed at least 70 cm above the burner. Pharmaceutical grade (German Pharmacopoeia DAB, Erg. B.6, no. 505033001, Lohmann) amorphous ferric orthophosphate with a SSA of 25 m² g⁻¹ served as reference compound for BET and XRD measurements. FePO₄-NPs for the human study were produced from stable isotope (⁵⁷Fe) enriched precursors, bulk FePO₄ and FeSO₄ from (⁵⁸Fe) enriched precursors (Chemgas). SSA was determined by N₂ adsorption (Micromeritics Tristar 3000, Micromeritics Instruments Corp) at 77 K in the relative pressure range $p/p_0 = 0.05–0.25$ and calculated using Brunauer–Emmett–Teller (BET) theory. Assuming dense spherical particles, the particle diameter (d_{BET}) was calculated from the measured SSA according to $d_{\text{BET}} = 6/(\rho \cdot \text{SSA})$, where ρ is

the solid particle density ($\text{FePO}_4 \cdot 2\text{H}_2\text{O} = 2.87 \text{ g cm}^{-3}$)⁴⁶. For transmission electron microscopy (TEM) analysis, the powders were deposited on a parlodion foil supported on a copper grid and analyzed on a CM12 microscope (FEI, LaB6 cathode, operated at an acceleration voltage of 100 kV). The crystallinity of the powders was investigated by X-ray diffraction (XRD) on a AXS D8 Advance diffractometer (Bruker) operating with a Cu-K α radiation. Hydrodynamic diameter was determined by dynamic light scattering using a Zetasizer Nano ZS (Malvern).

Animal studies. *Intestine-specific DMT1 knockdown (DMT1^{int/int}) model.* Intestine-specific DMT1 knockdown (DMT1^{int/int}) mice were bred by crossing floxed DMT1 (DMT1^{fl/fl}) mice on a homogenous C57BL/6 strain (courtesy of Nancy Andrews, Duke University, USA²¹) with villin-Cre transgenic mice on the C57BL/6J strain (ETH Zurich). The floxed DMT1 mice were back-crossed to a C57BL/6J background for six generations to establish the DMT1^{fl/fl} mouse breeding colony at ETH Zurich. The 6th generation was then shipped to the Vivarium at NWU to establish the intestine-specific DMT1 knockdown and villin-Cre mouse breeding colony for the experiments described in this article. To obtain DMT1^{int/int} mice, the animals needed to be homozygously floxed and have the villin-Cre transgene (Cre-positive). The homozygously floxed littermates (DMT1^{fl/fl}) that did not have the villin-Cre transgene (Cre-negative) served as control in all mice experiments to account for a potential effect of floxing on iron absorption and biodistribution. To breed these mice, we mated heterozygously floxed males that have the villin-Cre (Cre-positive) transgene with homozygously floxed females without the villin-Cre transgene (Cre-negative). Theoretically, this results in an approximate yield of 25% DMT1 KO and 25% controls per litter. In order to obtain the required number of mice for the different experiments, we continuously bred, genotyped and enrolled mice into the experiments. Thus, mice in the different experimental groups are from different litters.

Genotyping. The genotyping method to screen each mouse bred from the floxed DMT1 and villin-Cre mice colony was as follows. Briefly, a tissue sample (distal tail sample [$\leq 2 \text{ mm}$]) was collected at PND 10–21⁴⁷. gDNA isolation was done using the GenElute™ Mammalian Genomic DNA (gDNA) Miniprep Kit (Sigma Aldrich) following the manufacturers protocol. The quality of DNA was assessed and quantified using the NanoDrop™ spectrophotometer (ND-1000, Wilmington, DE, USA). Gene specific polymerase chain reaction (PCR) was performed and amplicons were visualized using ethidium bromide stained gel electrophoresis. For PCR amplification of the DMT1 gene the forward primer 5'-atggcgagtagaggctt-3' and the reverse primer 5'-cctgcatgcagaac-caatg-3' were used. For PCR amplification of the villin-Cre gene the forward primer 5'-gtgtgggacagagaacaaacc-3' and reverse primer 5'-acatctcagttctgctgg-3' were used together with an endogenous control (MyD88) primer pair 5'-agacaggctgagtgcaactgtgctg-3' and 5'-ccggcaactagaaacagacagactatcg-3'. Control gDNA with known genotype (ETH) as well as none-template control samples were included in each PCR run.

Housing and diets. Mice (for breeding and in experiments) were housed in polysulfone individually ventilated cages (391 × 199 × 160 mm [W × D × H]) (Tecniplast, UK) with Alpha-Dri® alpha cellulose bedding (Alpha-Dri, Shepherd Speciality Papers) (<2.00 ppm iron) under a 12/12 h light/dark cycle (lights on at 06:00) at 22 ± 2 °C and 55 ± 10% relative humidity. The diets used in the experiments and for breeding of experimental mice were commercially obtained purified diets according to AIN93-G standard⁴⁸, with modifications in iron content and compound. Iron fortified diets contained 35 mg iron per kg (ppm) diet, while iron deficient reference diets contained 3 ppm iron (native iron only). The diets were produced by Dyets Inc. (2508 Easton Avenue, P. O. Box 3485, Bethlehem, PA 18017, USA). Iron content of diets was analyzed in spot samples from each batch by Covance Laboratory Services (Madison, WI, USA) before shipping. All mice had ad libitum access to food and to deionized water (18 mΩ). Mice were weighed three times per week (or more frequently during experiments) to monitor weight gain.

Ethics. All animal experiments were approved by the Animal Ethics Committee of the Faculty of Health Sciences of the North-West University (NWU-00050-16-A5 & NWU-00258-17-A5), Potchefstroom, South Africa, and were conducted following the 3R principles for animal research and the Animals in Research: Reporting In Vivo Experiments (ARRIVE) guidelines⁴⁹.

Characterization of intestine-specific DMT1 knockdown model. A total of 10 DMT1^{int/int} (n=6 male; n=4 female) and 21 DMT1^{fl/fl} (n=10 male, n=11 female) mice, born to dams that were kept on the purified AIN-93G diet containing 35 ppm iron (as ferrous citrate) ad libitum, were randomly allocated in pairs to receive an iron deficient (3 ppm native iron) or iron-sufficient (35 ppm ferrous citrate) diet ad libitum from PND 24 to PND 42. PND 42 was set as endpoint, as this was the time point when first mice reached an Hb < 4 g dL⁻¹, which we defined as humane endpoint²² (a humane endpoint is the earliest scientifically justified point at which pain or distress in an experimental animal can be prevented, terminated, or relieved, while meeting the scientific aims and objectives of the study⁵⁰). Hemoglobin (Hb) concentrations were measured in tail blood spots (20 µg dL⁻¹) at PND 24, 27, 30, 33, 36, 39 and 42 using a calibrated Hb 201 + HemoCue® system (HemoCue Angelholm, Sweden). At PND 42, mice were euthanized by decapitation, and liver, duodenum and colon tissue immediately removed, snap frozen in liquid nitrogen, and stored at -80 °C until analysis.

Expression of DMT1 mRNA harboring an iron-responsive element (IRE) in its 3'-terminal exon and the upstream 5' exon1A in duodenum, colon and liver was analyzed with qPCR. PCR ready Syber green primers were synthesized by IDT (WhiteHead Scientific, South Africa). Primer pair sequences were adapted from Hubert and Hentze (2002)²³. Total RNA was isolated by using Trizol reagent following the standardized protocol. cDNA synthesis was performed using 10 mM oligo-dT_{18mer} and random hexamer primer mix with Superscript II reverse transcriptase (Qiagen), following the method prescribed by the manufacturer. A total of 50 ng cDNA was used

as template in triplicate qPCR reactions with QuantiNova sybr green 2× master mix together with 1 mM syber green ready primers. Reactions were prepared and amplification was performed at 94 °C for 20 s, 55 °C at 40 s and 72 °C at 30 s for 30 cycles. Gene expression was deduced using 18S and β Actin as endogenous reference genes to calculate delta Ct values for further statistical analysis.

Eighteen-day FePO₄-NP feeding study in DMT1^{int/int} and DMT1^{fl/fl} mice. A total of 15 DMT1^{int/int} (n=6 male; n=9 female) and 13 DMT1^{fl/fl} (n=6 male, n=7 female) mice, born to dams that were kept on the standardized AIN-93 G diet containing 35 ppm iron (as ferrous sulphate [FeSO₄]) ad libitum, were randomly allocated in pairs to receive a diet fortified with 35 ppm FePO₄-NP (SSA 98 m²g⁻¹) or FeSO₄ (reference compound) added to an iron-free AIN93-G diet from PND 24 to PND 42 ad libitum. Hb concentrations were measured in tail blood spots at PND 24, 27, 30, 33, 36 and 42 using the Hb 201 + HemoCue[®] system (HemoCue Angelholm, Sweden). At PND 42, mice were euthanized by decapitation and liver tissue immediately removed, snap frozen in liquid nitrogen, and stored at -80 °C until analysis.

Liver tissue samples were homogenized and digested with nitric acid according to Erikson et al. (1997)⁵¹, and total iron concentrations were measured by using the hydrogen reaction mode on an Agilent 7900 quadrupole ICP-MS at the Central Analytical Facilities, Stellenbosch University, South Africa. Samples were introduced via a 0.4 ml/min micromist nebulizer into a peltier-cooled spray chamber at a temperature of 2 °C. The instrument was optimized for analysis in high matrix introduction (HMI) mode, and all samples and standards were diluted with argon gas to minimize matrix load to the analyzer. The instrument was calibrated using a National Institute of Standards and Technology (NIST) traceable standard (Inorganic Ventures, USA). NIST-traceable quality control standards at high and low concentration levels (De Bruyn Spectroscopic Solutions, Bryanston, South Africa) were analyzed to verify the accuracy of the calibration before sample analysis commenced and this was repeated for every 12 samples to monitor drift. A germanium (Ge) internal standard was introduced online to monitor instrument drift and correct for matrix differences between samples and standards. During the course of the analysis, internal standard recovery was between 90 and 110% for all samples, and recovery for drift monitor standards between 95 and 105%. Oxide formation was less than 0.3%. Three replicate measurements were completed for each sample.

Absorption and biodistribution of radiolabeled FePO₄-NP and FeSO₄ from an acute oral dose in iron deficient anemic DMT1^{int/int} and DMT1^{fl/fl} mice. A total of 13 DMT1^{int/int} (n=7 male; n=5 female) and 15 DMT1^{fl/fl} (n=7 male, n=8 female) mice, born to dams that were kept on the standardized AIN-93 G diet containing 35 ppm iron (as FeSO₄) ad libitum, were placed on an iron deficient diet (3 ppm native iron) from PND 21 and throughout the entire experiment. Mice were randomly allocated to receive radiolabeled FePO₄-NP (SSA 98 m²g⁻¹) or FeSO₄. At PND 24, mice were transported to the South African Nuclear Energy Corporation South Africa (NECSA) and left to acclimatize to the new environment until administration of radiolabeled FePO₄-NP or FeSO₄ by oral gavage at PND 30 (29–31). The day before compound administration, Hb was measured in a tail blood spot.

Mice were fasted for 2 h before administration of the oral gavage during which they were acclimatized to metabolic cages (3701M081; Tecniplast). Then, a single dose of ~50 μ g iron in the form of the allocated compound labelled with ⁵⁹Fe (mean activity: 0.30 MBq) was orally gavaged (in 100 μ L saline containing 0.1% bovine serum albumin) using disposable flexible gavage needles. Total dose administered was determined by measuring syringe activity before and after gavage using a dose calibrator (Capintec CRC-15R, Capintec Inc., Ramsey, NJ, USA). Mice were then placed into a clean metabolic cage and received ad libitum access to iron deficient diet (3 ppm iron) one hour after oral gavage. After 24 h, the mice were euthanized by decapitation and the following individual organs were dissected and analyzed for ⁵⁹Fe content and weighed using an automated Hidex[®]600 SL gamma-counter (Hidex Oy, Finland). All counts were adjusted for decay: whole blood, heart, lung, liver, spleen, stomach, duodenum, peyer's patches, ileum, jejunum, colon, kidneys, femur, as well as feces and urine. Chyme was separated from the intestinal segments by washing with 1% phosphate-buffered saline.

A total of 15 mg of the nanostructured FePO₄ (SSA 98 m²g⁻¹) was irradiated in the SAFARI-1 20 MW research reactor in a hydraulic position at a neutron flux of 1 × 10¹⁴ n/cm²s for 16 days with a 3 day cooling period. Irradiation provided 512 MBq ⁵⁹Fe (t_{1/2} = 44.5 days) per 1 mg of FePO₄-NPs⁵². The color of the FePO₄-NP (SSA 98 m²g⁻¹) remained yellowish during the irradiation given confidence that the particles retained their nano structure. This was further confirmed by measuring the surface area using a Tristar 3000 BET surface area and porosity analyzer (Micromeritics, Norcross, USA). Using a special small volume adapter the SSA of the irradiated particles was determined to be 79.1 m²g⁻¹ which mimicked the SSA determined prior to irradiation. Special care was taken to remove the static nature of the NP after irradiation using a Antistatic Ionizer (RADAWG, Radom, Poland), before opening and during handling of the radioactive labelled NPs. FePO₄-NP were decayed a further 30 days prior to animal administration to allow for the co-activated ³²P (t_{1/2} = 14 days) to decay. ³²P is a pure β emitter and hence did not interfere with the determination using gamma spectrometry at the > 1000 keV range⁵². ⁵⁹Fe-labelled FeSO₄ was purchased from American Radiolabelled Chemicals, Inc. (St. Louis, USA) with a specific activity > 185 GBq/g. In order to mimic the chemical administered dose used for the NP's (50 μ g and 0.3 MBq), non radioactive FeSO₄ was added to a subset of the purchased stock solution. ⁵⁹Fe radioactivity (for administration) was detected by a dose calibrator (Capintec CRC-15R, Capintec Inc., Ramsey, NJ, USA), while samples were analyzed using an automated Hidex[®]600 SL gamma-counter (Hidex Oy, Finland) making use of the 1099 keV 56.5% gamma emission. Cross calibration between the two instruments were obtained by using a ⁵⁹Fe standard curve after a series of dilutions. The irradiated particles were dispersed in saline containing 0.1% bovine serum albumin by mixing for 30 s on a vortex followed by sonication for 10 min in a Sonorex Digitec waterbath (Bandelin Electronic) at 35 kHz and 80 W and were gavaged within 15 min after sonication. We acknowledge that we did not determine absorption and biodistribution of FePO₄-NP with an SSA of 188 m²g⁻¹ in our mouse

experiments because we were not able to radio-label this compound without colour and structural changes (visual inspection) after irradiation in the reactor as opposed to the $98 \text{ m}^2 \text{ g}^{-1}$ where this was not observed.

Statistical analysis. Data were analyzed using IBM SPSS Statistics software (version 24). Data were examined for normality of distribution (using q–q plots, histograms, and Shapiro–Wilk test) and the presence of outliers (using box plots). Homogeneity of variance was examined by the Levene's test. Variables that significantly deviated from normality and/or variance of homogeneity were transformed prior to inferential statistical analysis. Differences in Hb trajectories over time (PND 24–42) by genotype (DMT1^{int/int} vs. DMT1^{fl/fl}) and by dietary iron content (35 ppm vs. 3 ppm) or iron compound (FePO₄-NT vs. FeSO₄) were determined using repeated measures ANOVA. Differences in tissue iron concentrations, gene expression and percentage initial ⁵⁹Fe dose/g tissue by genotype and by iron compound were determined by two-sided independent t-tests. The results were expressed as means ± SEM and differences were considered significant at $p < 0.05$.

Human study. Design and subjects. In a randomized cross-over study, iron deficient, mostly anemic Thai women ($n = 18$) aged 18 to 49 years consumed four test meals containing ⁵⁷Fe-labeled FePO₄-NP (SSA $98 \text{ m}^2 \text{ g}^{-1}$), ⁵⁷Fe-labeled FePO₄-NP (SSA $188 \text{ m}^2 \text{ g}^{-1}$), ⁵⁸Fe-labeled bulk FePO₄ (negative reference compound) and ⁵⁸Fe-labeled FeSO₄ (positive reference compound) in random order (using a computerized random number generator—Excel). Stable iron isotope incorporation in red blood cells was determined 14 days after test meal administration.

Women were eligible to participate in the study if: (1) female aged 18 to 49 years; (2) body mass index (BMI) $< 23 \text{ kg/m}^2$ and body weight $< 65 \text{ kg}$; (3) Hb $\geq 80 \text{ g/L}$ and plasma ferritin $< 25 \text{ } \mu\text{g/L}$; (4) not pregnant (confirmed by pregnancy test) or lactating; (5) healthy, no chronic diseases or medications (except oral contraceptives) and no inflammation (C-reactive protein (CRP) $< 5 \text{ mg/L}$); (6) no blood donation or significant blood loss at least 4 months before study start; (7) no consumption of vitamin or mineral supplements at least 2 weeks before study start; (8) normal hemoglobin A (HbA) or HbE trait; and (9) nonsmokers.

Sample size calculations indicated that 16 women should be included based on 80% power to detect a 40% difference in iron bioavailability within subjects, an SD of 8.2% for log-transformed absorption data from previous absorption studies with the same meal and iron source/compound in a similar population of Thai women, and a type I error rate of 5%. We anticipated a dropout rate of 10% and therefore recruited 18 women.

Ethics. The study has been carried out according to the guidelines laid down in the Declaration of Helsinki, and all procedures involving human study participants were approved by the Ethics Committee of ETH Zurich (Zurich, Switzerland) and the Mahidol University Central Institutional Review Board (Salaya, Nakhon Pathom, Thailand). The study was registered at clinicaltrials.gov as NCT03660462 on 06/11/2018. Detailed oral and written information explaining the study purposes and potential risks and benefits were provided to the interested volunteers. Written informed consent was obtained from all participants. The oral administration of stable isotopes does not present any health risk. All data were coded and treated confidentially.

Study procedures. Women were recruited by screening at the Institute of Nutrition at Mahidol University and at the Khlong Yong Health Promoting Hospital in Nakhon Pathom, Thailand. All details of the study were explained to them, and if they were interested in participating in the study, they were asked to sign the written informed consent form. Then, weight and height were measured (to calculate BMI), and a venous blood sample collected to determine Hb, serum ferritin, and C-reactive protein concentrations. Women who fulfilled all the inclusion criteria were instructed to not eat red meat, fish or poultry four days prior to the scheduled test meals.

In a first phase, the women consumed two randomly assigned test meals (A, B, C or D) between 7.00 and 9.00 am after an overnight fast on study day 1 and 2. In the second phase, the women consumed the remaining randomly assigned test meals (A, B, C or D) between 7.00 and 9.00 am after an overnight fast on day 16 or 17. To distinguish between the absorption of the two forms of ⁵⁷Fe-labeled FePO₄-NP (SSA $98 \text{ m}^2 \text{ g}^{-1}$ and SSA $188 \text{ m}^2 \text{ g}^{-1}$) and between ⁵⁸Fe-labeled FeSO₄ and FePO₄, the subjects consumed one Fe compound labeled with ⁵⁷Fe and one with ⁵⁸Fe in each phase. The test meals (see details below) were fortified with 2 mg of the respective isotopically labelled iron compound and administered with a glass of deionized water (200 ml). Fourteen days after the last test meal administration in the first phase (day 16) and again fourteen days after the last test meal administration in the second phase (day 31), a venous blood sample was taken to determine iron absorption.

Composition of the test meal. The test meal was composed of steamed white rice (50 g dry weight), which was served with a vegetable soup prepared from local vegetables (50 g white cabbage, 50 g Chinese cabbage, 30 g Thai mushrooms and 20 g steamed carrots) in 120 mL of water. All ingredients were purchased in bulk and used for the entire study. The food portions were kept frozen until use, and each portion was microwaved on the day of feeding.

Stable-isotope labels. ⁵⁸FeSO₄ were prepared from ⁵⁸Fe-enriched elemental iron ($> 99.8\%$ isotopic enrichment; Chemgas) by dissolution in 0.1 mol/L sulfuric acid. ⁵⁸FePO₄ was prepared from ⁵⁸Fe-enriched elemental iron ($> 99.8\%$ isotopic enrichment; Chemgas). The two FePO₄-NP (SSA $98 \text{ m}^2 \text{ g}^{-1}$ and $188 \text{ m}^2 \text{ g}^{-1}$) were prepared from ⁵⁷Fe-enriched elemental iron ($> 99.8\%$ isotopic enrichment; Chemgas) by flame spray pyrolysis as described previously⁵. We analyzed the labeled iron compounds for iron isotopic composition and the tracer iron concentration via isotope-dilution mass spectrometry as described below.

Laboratory analyses. Venous blood samples were drawn into EDTA-treated tubes. We measured Hb immediately after blood draw with the use of hematology analyzer (Sysmex, Kobe, Japan) and quality controls provided by the manufacturer before each assessment. Hemoglobin typing for β -globin abnormality was done by using HPLC (Variant Hemoglobin Testing System; BioRad, Hercules, CA) with calibrators and controls provided by the manufacturer. DNA analysis for α -globin abnormalities was done by using a GeneAmp PCR System (Applied Biosystem, Foster City, CA) and a Gel Doc 2000 Gel Documentation System (BioRad, Hercules, CA). A 500 μ L aliquot of whole blood was frozen for isotopic analysis (see below). The remaining blood was centrifuged and the plasma aliquoted and stored at -20°C . Whole blood and plasma were shipped frozen to the ETH Zurich, Switzerland, for analysis of iron (plasma ferritin and soluble transferrin receptor) and inflammation (C-reactive protein, alpha-1-acid glycoprotein) parameters using a multiplex immunoassay⁵³. Anemia was defined as Hb < 120 g/L⁵⁴. Iron deficiency was defined as plasma ferritin < 12 mg/L and/or soluble transferrin receptor > 8.3 $\mu\text{g}/\text{mL}$ ⁵³, and iron deficiency anemia was defined as Hb < 120 g/L⁵⁴ and plasma ferritin < 12 mg/L and/or soluble transferrin receptor concentration > 8.3 $\mu\text{g}/\text{mL}$ ⁵³. Normal C-reactive protein and alpha-1-acid glycoprotein concentrations for this assay in healthy adults are < 5 mg/L and < 1 g/L, respectively⁵³.

Calculation of iron absorption. Whole blood samples were mineralized in duplicate with the use of a nitric acid and microwave digestion followed by separation of the iron from the blood matrix via anion-exchange chromatography and a subsequent precipitation step with ammonium hydroxide. We measured iron isotope ratios by using an inductively coupled plasma mass spectrometer (Neptune, Thermo Finnigan, Germany) equipped with a multicollector system for simultaneous iron beam detection⁵⁵. We calculated the amounts of ⁵⁷Fe and ⁵⁸Fe isotopic labels in blood 14 days after administration of the test meals based on the shift in iron-isotopic ratios and the estimated amount of iron circulating in the body. We remeasured the baseline isotopic composition in blood at the start of the second phase of test meals. Circulating iron was calculated based on the blood volume that was estimated from body length and weight at endpoint measurement according to Linderkamp et al.⁵⁶ and measured Hb (mean Hb from baseline and endpoint). The calculations were based on the methods described by Turnlund et al.⁵⁷ and Cercamondi et al.⁵⁸, taking into account that iron isotopic labels are not monoisotopic.

Data and statistical analysis. Data were analyzed using SPSS (IBM SPSS statistics, version 22.0). Normally distributed data were presented as mean \pm SD, and not normally distributed data as median (IQR). Repeated-measures ANOVA was used to assess the effect of iron compound on square root-transformed fractional iron absorption. Fractional iron absorption was the dependent variable and the iron compound was added to the model as the independent variable; pairwise comparisons were performed using two-sided paired t-tests with Bonferroni adjustment for multiple testing. Separate linear regressions were done to compare predictors of iron absorption from the nano-sized iron compounds and the bulk sized compounds. C-reactive protein and serum ferritin (iron status) were added as independent variables with the dependent variable being (1) iron absorption from bulk FePO₄ and FeSO₄ and (2) iron absorption from the two FePO₄-NPs. Significance was set at $P < 0.05$.

Data availability

All relevant data are included in the manuscript. These are also available by the authors upon request.

Received: 1 September 2021; Accepted: 20 January 2022

Published online: 18 February 2022

References

- Burke, R. M., Leon, J. S. & Suchdev, P. S. Identification, prevention and treatment of iron deficiency during the first 1000 days. *Nutrients* **6**(10), 4093–4114 (2014).
- Zimmermann, M. B. & Hurrell, R. F. Nutritional iron deficiency. *Lancet* **370**(9586), 511–520 (2007).
- Hurrell, R. F. Fortification: overcoming technical and practical barriers. *J. Nutr.* **132**(4 Suppl), 806s–812s (2002).
- Zimmermann, M. B. & Hilty, F. M. Nanocompounds of iron and zinc: their potential in nutrition. *Nanoscale* **3**(6), 2390–2398 (2011).
- Hilty, F. M. *et al.* Iron from nanocompounds containing iron and zinc is highly bioavailable in rats without tissue accumulation. *Nat. Nanotechnol.* **5**(5), 374–380 (2010).
- Forbes, A. L. *et al.* Comparison of in vitro, animal, and clinical determinations of iron bioavailability: International Nutritional Anemia Consultative Group Task Force report on iron bioavailability. *Am. J. Clin. Nutr.* **49**(2), 225–238 (1989).
- McConnell, E. L., Basit, A. W. & Murdan, S. Measurements of rat and mouse gastrointestinal pH, fluid and lymphoid tissue, and implications for in-vivo experiments. *J. Pharm. Pharmacol.* **60**(1), 63–70 (2008).
- Sangkhae, V. & Nemeth, E. Regulation of the iron homeostatic hormone hepcidin. *Adv. Nutr. (Bethesda, Md)* **8**(1), 126–136 (2017).
- McKie, A. T. The role of Dcytb in iron metabolism: An update. *Biochem. Soc. Trans.* **36**, 1239–1241 (2008).
- McKie, A. T. & Simpson, R. J. Intestinal iron absorption. In *Iron physiology and pathophysiology in humans* (eds Anderson, G. J. & McLaren, G. D.) 101–116 (Springer, 2012).
- Hentze, M. W., Muckenthaler, M. U., Galy, B. & Camaschella, C. Two to tango: Regulation of mammalian iron metabolism. *Cell* **142**(1), 24–38 (2010).
- Aslam, M. F. *et al.* Ferroportin mediates the intestinal absorption of iron from a nanoparticulate ferritin core mimetic in mice. *FASEB J.* **28**(8), 3671–3678 (2014).
- Pereira, D. I. A. *et al.* Caco-2 cell acquisition of dietary iron(III) invokes a nanoparticulate endocytic pathway. *PLoS ONE* **8**(11), e81250 (2013).
- Perfecto, A. *et al.* Mechanisms of iron uptake from ferric phosphate nanoparticles in human intestinal Caco-2 cells. *Nutrients* **9**(4), 113 (2017).
- Rudin, T. & Pratsinis, S. E. Homogeneous iron phosphate nanoparticles by combustion of sprays. *Ind. Eng. Chem. Res.* **51**(23), 7891–7900 (2012).
- Strobel, R. & Pratsinis, S. E. Flame aerosol synthesis of smart nanostructured materials. *J. Mater. Chem.* **17**(45), 4743–4756 (2007).

17. Wegner, K. & Pratsinis, S. E. Scale-up of nanoparticle synthesis in diffusion flame reactors. *Chem. Eng. Sci.* **58**(20), 4581–4589 (2003).
18. Hallberg, L., Rossander-Hulthén, L. & Gramatkovski, E. Iron fortification of flour with a complex ferric orthophosphate. *Am. J. Clin. Nutr.* **50**(1), 129–135 (1989).
19. von Moos, L. M. *et al.* Iron phosphate nanoparticles for food fortification: Biological effects in rats and human cell lines. *Nanotoxicology* **11**(4), 496–506 (2017).
20. Faria, M. *et al.* Minimum information reporting in bio-nano experimental literature. *Nat. Nanotechnol.* **13**(9), 777–785 (2018).
21. Gunshin, H. *et al.* Slc11a2 is required for intestinal iron absorption and erythropoiesis but dispensable in placenta and liver. *J. Clin. Invest.* **115**(5), 1258–1266 (2005).
22. Koziol, B. J., Ohira, Y., Edgerton, V. R. & Simpson, D. R. Changes in work tolerance associated with metabolic and physiological adjustment to moderate and severe iron deficiency anemia. *Am. J. Clin. Nutr.* **36**(5), 830–839 (1982).
23. Hubert, N. & Hentze, M. W. Previously uncharacterized isoforms of divalent metal transporter (DMT)-1: Implications for regulation and cellular function. *Proc. Natl. Acad. Sci. U S A* **99**(19), 12345–12350 (2002).
24. Hotz, K. & Walczyk, T. Natural iron isotopic composition of blood is an indicator of dietary iron absorption efficiency in humans. *J. Biol. Inorg. Chem.* **18**(1), 1–7 (2013).
25. World Health Organisation. Global health observatory data repository: Prevalence of anaemia in women of reproductive age estimates by country. <https://apps.who.int/gho/data/view.main.ANAEMIAWOMENPREVANEMIA>. Accessed October 2021.
26. Kim, H. J. *et al.* Cytotoxicity, intestinal transport, and bioavailability of dispersible iron and zinc supplements. *Front. Microbiol.* **8**, 749 (2017).
27. Theil, E. C. *et al.* Absorption of iron from ferritin is independent of heme iron and ferrous salts in women and rat intestinal segments. *J. Nutr.* **142**(3), 478–483 (2012).
28. Gehrke, H. *et al.* In vitro toxicity of amorphous silica nanoparticles in human colon carcinoma cells. *Nanotoxicology* **7**(3), 274–293 (2013).
29. McCracken, C., Zane, A., Knight, D. A., Dutta, P. K. & Waldman, W. J. Minimal intestinal epithelial cell toxicity in response to short- and long-term food-relevant inorganic nanoparticle exposure. *Chem. Res. Toxicol.* **26**(10), 1514–1525 (2013).
30. Schübbe, S. *et al.* Size-dependent localization and quantitative evaluation of the intracellular migration of silica nanoparticles in Caco-2 cells. *Chem. Mater.* **24**(5), 914–923 (2012).
31. Gerloff, K., Albrecht, C., Boots, A. W., Förster, I. & Schins, R. P. F. Cytotoxicity and oxidative DNA damage by nanoparticles in human intestinal Caco-2 cells. *Nanotoxicology* **3**(4), 355–364 (2009).
32. Mu, Q. *et al.* Mechanism of cellular uptake of genotoxic silica nanoparticles. *Part Fibre Toxicol.* **9**(1), 29 (2012).
33. Sharma, V., Singh, P., Pandey, A. K. & Dhawan, A. Induction of oxidative stress, DNA damage and apoptosis in mouse liver after sub-acute oral exposure to zinc oxide nanoparticles. *Mutation Res./Genetic Toxicol. Environ. Mutagenesis* **745**(1), 84–91 (2012).
34. Trouiller, B., Reliene, R., Westbrook, A., Solaimani, P. & Schiestl, R. H. Titanium dioxide nanoparticles induce DNA damage and genetic instability in vivo in mice. *Cancer Res.* **69**(22), 8784–8789 (2009).
35. Park, E. J. *et al.* A 13-week repeated-dose oral toxicity and bioaccumulation of aluminum oxide nanoparticles in mice. *Arch. Toxicol.* **89**(3), 371–379 (2015).
36. van der Zande, M. *et al.* Sub-chronic toxicity study in rats orally exposed to nanostructured silica. *Part Fibre Toxicol.* **11**(1), 8 (2014).
37. Moreno-Olivas, F., Tako, E. & Mahler, G. J. ZnO nanoparticles affect nutrient transport in an in vitro model of the small intestine. *Food Chem. Toxicol.* **124**, 112–127 (2019).
38. Rohner, F. *et al.* Synthesis, characterization, and bioavailability in rats of ferric phosphate nanoparticles. *J. Nutr.* **137**(3), 614–619 (2007).
39. Srinivasu, B. Y. *et al.* Beneficiary effect of nanosizing ferric pyrophosphate as food fortificant in iron deficiency anemia: Evaluation of bioavailability, toxicity and plasma biomarker. *RSC Adv.* **5**(76), 61678–61687 (2015).
40. Yun, J.-W. *et al.* Comparative toxicity of silicon dioxide, silver and iron oxide nanoparticles after repeated oral administration to rats. *J. Appl. Toxicol.* **35**(6), 681–693 (2015).
41. Garcia-Fernandez, J. *et al.* In vitro and in situ experiments to evaluate the biodistribution and cellular toxicity of ultrasmall iron oxide nanoparticles potentially used as oral iron supplements. *Nanotoxicology* **14**(3), 388–403 (2020).
42. Shafie, E. H. *et al.* The effects of nanoparticles containing iron on blood and inflammatory markers in comparison to ferrous sulfate in anemic rats. *Int. J. Prev. Med.* **7**, 117–117 (2016).
43. Shen, Y. *et al.* Amyloid fibril systems reduce, stabilize and deliver bioavailable nanosized iron. *Nat. Nanotechnol.* **12**(7), 642–647 (2017).
44. Rehman, H. *et al.* Effect of endoxylanase and iron oxide nanoparticles on performance and histopathological features in broilers. *Biol. Trace Elem. Res.* **193**(2), 524–535 (2020).
45. Mädler, L., Stark, W. J. & Pratsinis, S. E. Flame-made ceria nanoparticles. *J. Mater. Res.* **17**(6), 1356–1362 (2011).
46. Perry DL. *Handbook of Inorganic Compounds*. (CRC Press, 2016).
47. Picazo, M. G. & García-Olmo, D. C. DNA from tissues of young mice is optimal for genotyping. *Electron. J. Biotechnol.* **18**(2), 83–87 (2015).
48. Reeves, P. G., Nielsen, F. H. & Fahey, G. C. Jr. AIN-93 purified diets for laboratory rodents: final report of the American Institute of Nutrition ad hoc writing committee on the reformulation of the AIN-76A rodent diet. *J. Nutr.* **123**(11), 1939–1951 (1993).
49. Kilkenny, C., Browne, W. J., Cuthill, I. C., Emerson, M. & Altman, D. G. Improving bioscience research reporting: The ARRIVE guidelines for reporting animal research. *PLoS Biol.* **8**(6), e1000412–e1000412 (2010).
50. Hendriksen, C., Cussleer, K., & Morton, D. Use of humane endpoints to minimise suffering. in *The COST Manual of Laboratory Animal Care and Use* (Howard, B., Bevalainen, T., Peratta, G. eds). (CRC Press, 2010).
51. Erikson, K. M., Pinero, D. J., Connor, J. R. & Beard, J. L. Regional brain iron, ferritin and transferrin concentrations during iron deficiency and iron repletion in developing rats. *J. Nutr.* **127**(10), 2030–2038 (1997).
52. Diehl, P. *Neutron Activation Calculator—WISE Uranium Project*. <http://www.wise-uranium.org/rnac.html>. Accessed 9 Feb 2015. (1995).
53. Erhardt, J. G., Estes, J. E., Pfeiffer, C. M., Biesalski, H. K. & Craft, N. E. Combined measurement of ferritin, soluble transferrin receptor, retinol binding protein, and C-reactive protein by an inexpensive, sensitive, and simple sandwich enzyme-linked immunosorbent assay technique. *J. Nutr.* **134**(11), 3127–3132 (2004).
54. WHO/UNICEF/UNU. *Iron Deficiency Anaemia Assessment, Prevention and Control*. (World Health Organization, 2001).
55. Hotz, K., Augsburger, H. & Walczyk, T. Isotopic signatures of iron in body tissues as a potential biomarker for iron metabolism. *J. Anal. At. Spectrom.* **26**(7), 1347–1353 (2011).
56. Linderkamp, O., Vermold, H., Riegel, K. & Betke, K. Estimation and prediction of blood volume in infants and children. *Eur. J. Pediatr.* **125**(4), 227–234 (1977).
57. Turnlund, J. R., Keyes, W. R. & Peiffer, G. L. Isotope ratios of molybdenum determined by thermal ionization mass spectrometry for stable isotope studies of molybdenum metabolism in humans. *Anal. Chem.* **65**(13), 1717–1722 (1993).
58. Cercamondi, C. I. *et al.* Total iron absorption by young women from iron-biofortified pearl millet composite meals is double that from regular millet meals but less than that from post-harvest iron-fortified millet meals. *J. Nutr.* **143**(9), 1376–1382 (2013).

Acknowledgements

We thank L von Moos, C Zeder, A Krzystek, C Blattmann, S Pratsinis (ETH Zurich, Switzerland), J Erhardt (Willstaett, Germany) for assistance in the production of the iron compounds, their characterization and laboratory and data analysis. We thank E Schraner (University of Zurich, Switzerland) for assistance with TEM. We thank K Venter (NWU, South Africa) for assistance in the execution of the animal experiments at NWU and Necsa. We thank J Gama (Necsa, South Africa) for the surface area determination of the irradiated NP and GS Smith (Necsa) for associated radiation protection making this possible. We thank the Thai women who participated in the study, and thank A Boonpraderm and S Rattarengsak (INMU, Thailand) for assistance with the test meals. This work was supported by the Swiss National Science Foundation (SNSF), National Research Program 64 “Opportunities and risks of nanomaterials”, no. 406440-141610; and ETH Zurich, Zurich, Switzerland.

Author contributions

The authors’ contributions were as follows—J.B., H.C.W., F.H., M.B.Z.: designed the study; H.C.W., S.G., S.T., P.M.: conducted the human study; J.B., H.C.W., L.Z., J.R.Z.: conducted the animal studies; H.C.W., J.B., L.Z., J.R.Z.: analyzed the data and performed the statistical analyses; all authors participated in the data interpretation; J.B., H.C.W., L.Z., M.B.Z.: wrote the first draft of the manuscript; and all authors edited the manuscript and read and approved the final version of the manuscript.

Funding

Swiss National Science Foundation (SNSF), National Research Program 64 “Opportunities and risks of nanomaterials”, no. 406440-141610; and ETH Zurich, Zurich, Switzerland.

Competing interests

The authors declare no competing interests.

Additional information

Supplementary Information The online version contains supplementary material available at <https://doi.org/10.1038/s41598-022-06701-x>.

Correspondence and requests for materials should be addressed to S.G. or M.B.Z.

Reprints and permissions information is available at www.nature.com/reprints.

Publisher’s note Springer Nature remains neutral with regard to jurisdictional claims in published maps and institutional affiliations.



Open Access This article is licensed under a Creative Commons Attribution 4.0 International License, which permits use, sharing, adaptation, distribution and reproduction in any medium or format, as long as you give appropriate credit to the original author(s) and the source, provide a link to the Creative Commons licence, and indicate if changes were made. The images or other third party material in this article are included in the article’s Creative Commons licence, unless indicated otherwise in a credit line to the material. If material is not included in the article’s Creative Commons licence and your intended use is not permitted by statutory regulation or exceeds the permitted use, you will need to obtain permission directly from the copyright holder. To view a copy of this licence, visit <http://creativecommons.org/licenses/by/4.0/>.

© The Author(s) 2022